Switchable pH-Responsive Polymeric Membranes Prepared *via* Block Copolymer Micelle Assembly

Suzana P. Nunes,[⊥,†] Ali Reza Behzad,[‡] Bobby Hooghan,[§] Rachid Sougrat,[‡] Madhavan Karunakaran,[⊥] Neelakanda Pradeep,[⊥] Ulla Vainio,[∥] and Klaus-Viktor Peinemann[⊥,*]

[‡]Imaging and Characterization Lab, [§]FEI, and [⊥]Advanced Membranes and Porous Materials Center at King Abdullah University of Science and Technology (KAUST), 23955-6900 Thuwal, Saudi Arabia, and [∥]HASYLAB at Deutsches Elektronen-Synchrotron (DESY), D-22607 Hamburg, Germany. [†] Present address: Water Desalination and Reuse Center at King Abdullah University of Science and Technology (KAUST), 23955-6900 Thuwal, Saudi Arabia.

ABSTRACT A process is described to manufacture monodisperse asymmetric pH-responsive nanochannels with very high densities (pore density $>2 \times 10^{14}$ pores per m^2), reproducible in m^2 scale. Cylindric pores with diameters in the sub-10 nm range and lengths in the 400 nm range were formed by self-assembly of metal-block copolymer complexes and nonsolvent-induced phase separation. The film morphology was tailored by taking into account the stability constants for a series of metal−polymer complexes and confirmed by AFM. The distribution of metal−copolymer micelles was imaged by transmission electron microscopy tomography. The pH response of the polymer nanochannels is the strongest reported with synthetic pores in the nm range (reversible flux increase of more than 2 orders of magnitude when switching the pH from 2 to 8) and could be demonstrated by cryo-field emission scanning electron microscopy, SAXS, and ultra/nanofiltration experiments.

KEYWORDS: micelle self-assembly · block copolymer · membrane · pH response

Films with regular monodisperse nanopores and ultrahigh porosity are needed in applications that vary from water purification[1] to sensors and information storage, as templates for nanowires[2] and scaffolds for tissue engineering, and for controlled drug delivery.[3] Commercial synthetic membranes for nanofiltration have been available for decades, but the pore size distribution is broad, leading to poor selectivity. Advanced technology for controlled drug release or analysis of biomolecules and other valuable solutes would profit from isoporous films, which respond to their environment, sensing changes in pH or small concentrations of analytes, acting as chemical gates.[4−6] Gluconic acid is a byproduct of the enzymatic oxidation of glucose. Aiming at diabetes therapy, pH-responsive pores can open or close to supply insulin, according to the depletion of glucose and acid production.[7] Innovative approaches for the development of stimuli-responsive membranes by functionalizing track-etched membranes have been recently reported. They have a narrow pore size distribution, but the porosity is very low.[8] Schacher *et al.* recently reported a pH-responsive block copolymer membrane with relatively broad pore size distribution.[9]

We report here a process to manufacture pH-responsive nanoporous films with very narrow pore size distribution, by combining the self-assembly of metal−block copolymer complexes and conventional methods of membrane production by phase inversion. We compare the influence of different metals on the final morphology, explore the exceptional pore regularity of the membrane, and demonstrate its particularly sharp response to pH.

Block copolymers have been previously explored to prepare nanoporous films, but in most cases the pores are obtained by dissolving one of the components of the film or by etching. The soluble component could be a homopolymer with the same composition as one of the blocks[3] or a strongly interacting small molecule.[10] Phillip *et al.* degraded lactide blocks by reaction with alkaline solutions to form pores.[11] Ozone has been used to etch isoprene blocks.[12]

The morphology of di- or triblock copolymers at thermodynamic equilibrium is driven by a balance of enthalpically unfavorable interactions between blocks and the entropic resistance of the chain to adopt extended configurations.[13] The phase diagram predicting the equilibrium morphologies is well known. However reaching equilibrium frequently requires long annealing times, and long-range order is not easy to obtain.

Attractive morphologies are found far from the thermodynamic equilibrium, and the big challenge is not only to direct the block copolymer assembly into the aimed structures but also to stabilize this state to

* Address correspondence to klausviktor.peinemann@kaust.edu.sa.

Received for review October 3, 2010 and accepted April 19, 2011.

Published online April 19, 2011
10.1021/nn200484v

produce the desired nanostructured film. Excellent reviews on the myriad of block copolymer assemblies in solution have been published.[14,15] We recently proposed the use of supramolecular assemblies of block copolymer micelles in solution in the presence of copper ions for the manufacture of skinned asymmetric membranes with a thin nanoporous top layer.[16] We extend here this idea to tailor a variety of morphologies for stimuli-responsive polymeric membranes using metal ions with different complexation strengths. Highly ordered structures were confirmed by atomic force microscopy. We used tomographic (transmission electron microscopy) imaging for the three-dimensional visualization of metal–copolymer micelles in the final membrane structure. We showed previously the response of water flux through the membrane to a changing pH.[16] Here we demonstrate a drastic increase in membrane selectivity with decreasing pH. The stimuli–response was imaged for the first time using cryo-scanning electron and environmental microscopy.

RESULTS AND DISCUSSION

Film Preparation and Morphology Characterization. Twenty wt % of polystyrene-*b*-poly (4-vinylpyridine) (PS-b-P4VP, 138,000-b-41,000 g/mol) block copolymer was dissolved in a mixture of 56/24 dimethyl formamide (DMF)/tetrahydrofuran (THF) containing 0.15 wt % acetates of copper(II), cobalt(II), nickel(II), and iron(II). Nanoporous films were formed after partial evaporation of THF, which is the most volatile solvent, followed by immersion in water, a nonsolvent for the block copolymer. DMF is a much better solvent for the pyridine block than for PS. Micelles are formed with PS cores, minimizing interaction with DMF, and hydrophilic P4VP coronas. Pyridine is known to form complexes with transition metals, and this is expected to contribute to the micelle stabilization.[18–20] Nanoporous asymmetric copolymer films were prepared by pyridine complexation with different metals under comparable conditions. The final surface morphology was analyzed by atomic force microscopy and can be seen in Figure 1. Besides stabilizing the individual micelle coronas, the metal ions promote the connectivity between P4VP chains of different micelles. The solution viscosity increases, and the whole assembly is stabilized. With partial evaporation of THF just before the immersion in water, the viscosity at the film top layer increases even more due to local increase of the polymer concentration. A fast solvent–water exchange finally leads to an abrupt decrease of chain mobility, and the morphology is completely frozen, giving rise to the ordered nanostructured membrane. Membranes prepared with copper ions were the most ordered, followed by nickel and cobalt. Films prepared with iron acetate have elongated or lamellar domains but do not have the characteristic pore morphology seen with other metal complexes. Films prepared with the same solvent

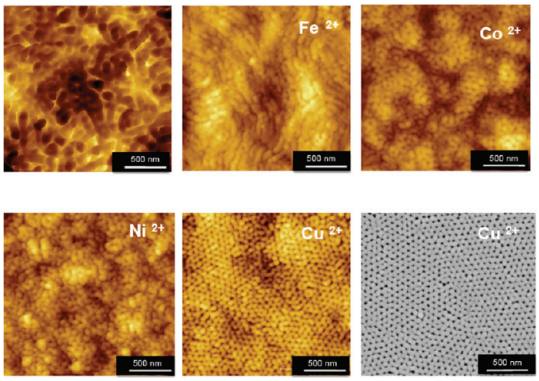

Figure 1. Atomic force microscopy (AFM) of membranes prepared from 20 wt % PS-b-P4VP in 56 wt % DMF and 24 wt % THF without and with 0.15 wt % of different metal acetates as complexing agents; on the bottom right is a cryo-scanning electron microscopy image of the membrane cast from solution with Cu^{2+}.

mixture, in the absence of metal, did not have an ordered morphology. Pyridine coordinates with metal ions through both σ-bonding and π-bonding. The stability constants (log K_1) for metal–pyridine complexes have been reported[19] as decreasing in the following order:

Cu(II) (2.52) > Ni(II) (1.78) > Co(II) (1.14) > Fe(II) (0.71)

This follows the Irving and Williams stability series of high-spin complexes formed by a ligand and divalent ions of transition metals.[20] Pyridine coordinates with transition metal ions through both σ- and π-bonding. The σ-bonds are formed with d-orbitals of the transition metal cations, leading to ligand field stabilization of the metal d-electrons. The magnitude of σ-bonding follows the same series as above, being stronger with Cu(II). The complex formation can be also seen as resulting from acid–base interactions between the basic ligand occupying sites in the first shell coordination sphere of the acid metal center.[21] The complex stability (and σ-bond strength) series reflects the state of order observed in the surface of the final nanoporous films in Figure 1. Stronger complexes stabilize the copolymer micelles and lead to ordered supramolecular structures. Cryo-scanning electron microscopy of a wet membrane surface is also shown in Figure 1 and confirms the highly ordered structure of the membrane with Cu^{2+}.

From the results with the series of metal ions, we understand that the form stability of the micelles and the intermicelle connection promoted by strong complexing agents are essential for the final morphology. When micelles are not stable enough, excessive mobility will lead to a chain rearrangement in the final stages of membrane formation without isoporous morphology.

The confirmation that micelles are kept intact and assembled as part of the final membrane morphology was possible by three-dimensional visualization through transmission electron microscopy tomography. A set of images is shown in Figure 2 for a membrane cast from a solution containing cobalt acetate. A tomography

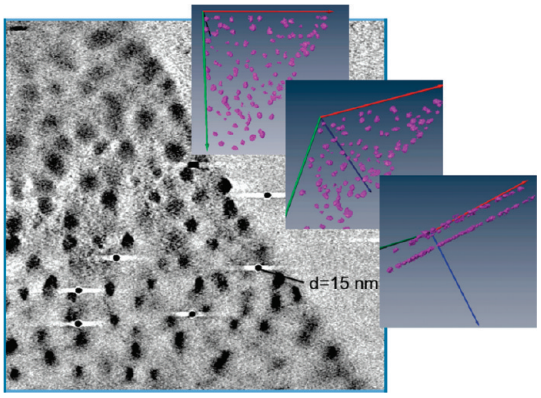

Figure 2. Transmission electron microscopy tomography of a PS-b-P4VP membrane cast from solution in DMF/THF/Co (acetate)$_2$ (tomography video in the Supporting Information). Details showing the membrane slice tilted at different angles, from top to bottom: 90° (orthogonal to the membrane surface), 45° and 0° (parallel to the surface). Small black spots: gold particles of 15 nm as size reference.

video is supplied in the Supporting Information. The presence of cobalt ion in the micelle corona gives rise to a strong contrast due to the high electron density (dark spots). Three pictures are shown depicting the distribution of micelles in a 150 nm membrane slice, which was tilted in different angles in the microscope. It is possible to see that particularly in one angle of observation the micelles are very regularly assembled. Two regular layers of micelles are observed constituting the slice.

pH-Dependent Flux Characterization. Fast one-step manufacture of membranes with very high porosity and homogeneous pore size without etching or any post-treatment, reproducible in large scale, is already a breakthrough, but even more attractive is the fact that the pores can be used as chemical gates without any further modification. Here we demonstrate the stimuli (pH) response of the films in the ultra/nanofiltration of polydisperse polyethylene glycol solutions, and we image the corresponding pore size change by using cryo-field emission electron microscopy, environmental microscopy, and SAXS. The membrane water flux as a function of pH is shown in Figure 3. A very sharp change of flux is measured between pH 4 and 6. The original flux values at extreme pH values (below 4 and above 7) are completely recovered, as shown in Figure 3a. In the middle pH range, the water flux values vary about 20% if the pH is increased or decreased. The cyclability of the membranes has to be confirmed at a large number of cycles. The very high flux at high pH is an order of magnitude larger than those measured for commercial track-etched membranes with similar pore size, demonstrating the exceptional porosity.[22]

The Hagen–Poiseuille equation gives an estimation of the effective pore size corresponding to the measured water flux through the membrane:

$$r = (8\eta LQ/\pi\Delta P)^{0.25}$$

where r is the pore radius, ΔP is the pressure drop through the membrane, η is the water viscosity, Q is the volumetric flow rate, and L is the length of the selective pores.

In Figure 3a the pore diameters estimated by the Hagen–Poiseuille equation are shown as a function of pH. The estimation assumes an effective pore length of 400 nm, which is the thickness of the ordered top layer of the membrane, as can be seen in Figure 3b, which is part of a focused ion beam (FIB) 3D reconstruction of the membrane pore structure. The reconstruction was obtained as reported before,[16] using the software Amira, after cutting 150 membrane slices by FIB. A pore density of 2.4×10^{14} pores per m^2 (based on electron scanning microscopy of the membrane surface) was used for calculation of the effective pore diameter.

The metal ion concentration added to the casting solution is enough to complex only 2–3 mol % of the pyridine groups. At low pH the free pyridine groups are protonated, leading to stretching of P4VP segments. Practically no hysteresis for water flux was observed by increasing and decreasing pH. This indicates that the process is reversible. The metal–copolymer interaction is strong enough to keep the physical cross-linking and stability of the micelle arrangement.

Figure 4 illustrates how the micelles assemble to form a pore and what happens at low pH values. As the pyridine groups are protonated, they become positively charged. The chains stretch due to charge repulsion and fill the space, which at high pH constitutes the pores. Guo *et al.* recently reported a dissipative particle dynamics simulation of pH-sensitive micelles with histidine residues due to protonation of the imidazole groups.[23] An analogous micelle expansion and contraction occurs in our system. Since the film morphology is directed by the micelle arrangement, the change in micelle dimensions gives rise to the changes of water flux.

A mixture of polyethylene glycol with nominal molecular weights 1500, 3000, 6000, 10 000, and 35 000 g/mol was used to evaluate the membrane selectivity. At high pH the membrane cutoff (smallest solute size with 90% retention) is above the molecular weight range tested. When the pH is decreased, the membrane becomes very selective (Figure 3c), retaining 90% of solutes with molecular weight around 6000 g/mol, which is in the range of a nanofiltration membrane.

The change of pore size under different pH values was confirmed using cryo-field emission scanning electron microscopy (cryo-FESEM) (Figure 5a) and environmental scanning electron microscopy (ESEM) (Figure 5b). By using ESEM a clear difference is observed between dry membranes and those wetted by aqueous solutions with different pH. A much clearer visualization was obtained by using cryo-FESEM. The effective pore size values, estimated by Hagen–Poiseuille

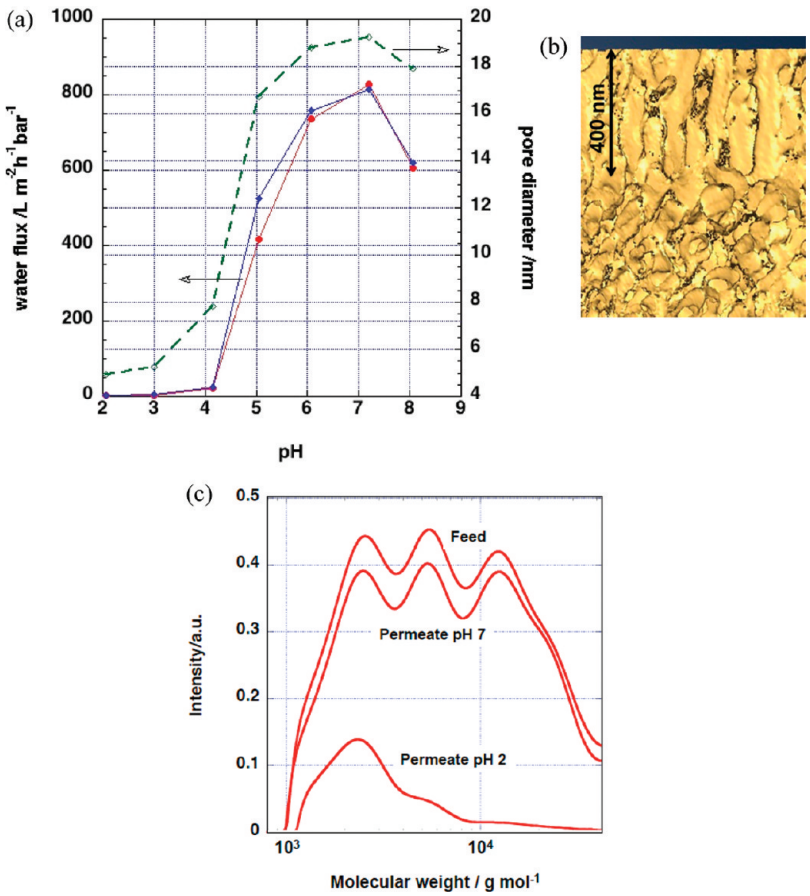

Figure 3. (a) Water flux measured with increasing pH from 2 to 10 (red) and decreasing back to 2 (blue); effective pore diameter was estimated by the Hagen–Poiseuille equation. (b) 3D reconstruction of membrane porosity after FIB microscopy: integrated asymmetric porous structure with ordered channels on the top (upper 400 nm) and larger disordered pores below. (c) Molecular weight distribution of polyethylene glycol solutions permeated through a membrane cast from 20 wt % PS-b-P4VP solution in 56 wt % DMF/24 wt % THF/0.15 wt % Cu(acetate)$_2$ measured at high and low pH.

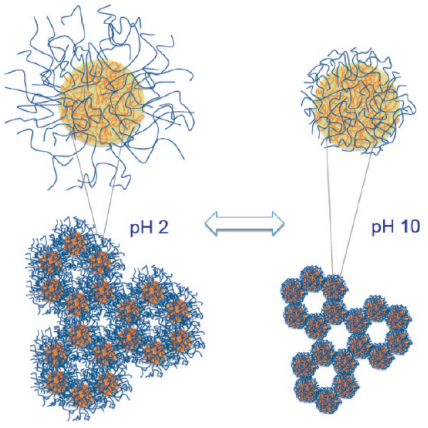

Figure 4. Micelle size change and assembly as a function of pH.

for high pH in Figure 3a, are very close to the pore sizes shown in the cryo-microscopy images in Figure 5a, which were around 21 nm. This confirms our assumption that the main flow resistance lies in the 400 nm thin ordered membrane top layer.

Figure 6 compares the SAXS analysis of the dry membrane and that of membranes immersed in different pH solutions. Details are presented in the Supporting information. The two-dimensional (2D) hexagonal morphology can be seen by SAXS analysis of dry membranes. A maximum in the scattering intensity is observed, followed by peaks of higher order, which fits a 2D hexagonal model. The distance between pore centers was estimated as 70.3 $\pm$ 0.4 nm. Now when immersed in solutions of pH 9 and 2, instead of sharp peaks characteristic of hexagonal ordering in the dry membrane, only one broad peak can be observed. At high pH, the peak width was found to be about 6-fold larger than that of the dry membrane, indicating significant structure distortion in the wetted membrane. The position of the first reflection is shifted, giving a characteristic length scale of 64 $\pm$ 2 nm for the membrane in high pH, slightly lower than for the dry state. When the membrane is immersed in a solution of low pH, the scattering intensity decreases substantially and a broad hump can be recognized only above q = 1 nm^{-1}, corresponding to much smaller structures. The power law exponent of -2 in the intensity can be interpreted to arise from remaining water channels that may have rather disordered lamellar morphologies,

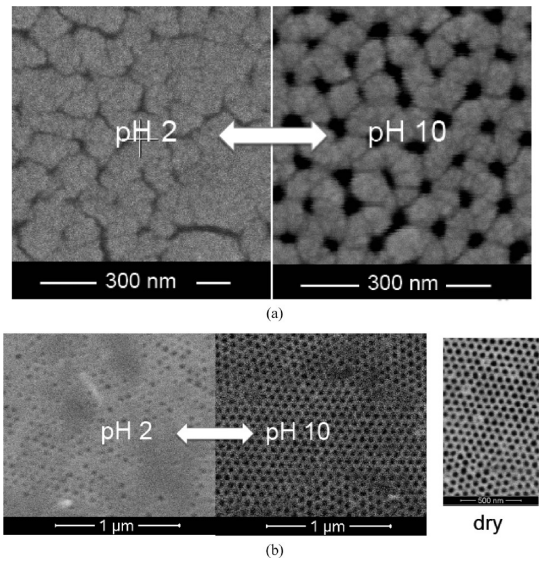

Figure 5. (a) Cryo-field emission scanning electron microscopy (Cryo-FESEM) and (b) environmental scanning electron microscopy (ESEM) of PS-b-P4VP membranes cast from solution in DMF/THF/Cu(acetate)$_2$, immersed in HNO_3 (pH 2) and NH_4OH (pH 10) aqueous solutions; (b, right) dry membrane observed by ESEM.

as indicated in Figure 5a. From the position of the hump, we may estimate these channels or lamellae to have widths of 1−3 nm.

The process reported here allows the preparation of large areas of asymmetric thin porous films on a nonwoven polymer using a technology that is conventionally applied for industrial production of ultrafiltration membranes.[24] Block copolymer membranes, which are 15 cm wide and 1 m long, have been prepared on polyester nonwoven. The membrane areas can be up-scaled, just by increasing the length of the nonwoven polyester. Low magnification scanning microscopy of a membrane prepared with copper

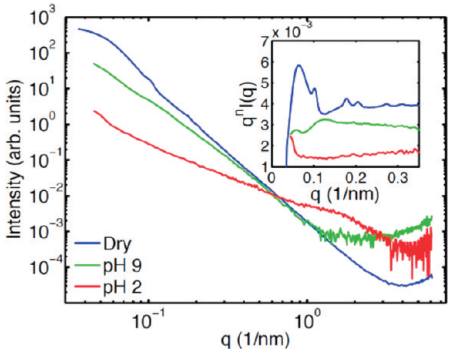

Figure 6. SAXS of PS-b-P4VP/Cu^{2+} nanoporous films in different environments: under vacuum (dry) and in aqueous solutions with pH 9 and 2. The inset shows the same intensities weighted with q^n (n = 2, 3.2, and 4 for pH 2, pH 9, and dry sample, respectively), where the differences in structures and the related power laws in the intensities can be better seen.

ions is supplied in the Supporting Information, demonstrating the long-range pore regularity.

CONCLUSION

Uniform polymeric nanochannels with diameters in the sub-10 nm range and lengths in the 400 nm range could be created by self-assembly of block copolymers in the presence of metal ions, followed by nonsolvent (water)-induced phase separation. The nanochannel order and density could be tailored by taking into account the stability constants for the metal−polymer complexes. The membrane morphology was characterized by AFM and TEM tomography. The sharp change of pore size as a function of pH with potential functionality as chemical gates has been demonstrated by cryo-FESEM, ESEM, and SAXS. This characteristic is allied to unusually high porosity and narrow pore size distribution. The manufacturing method can be easily up-scaled, by applying conventional technology of membrane production.

MATERIALS AND METHODS

Membrane Preparation. Polystyrene-*b*-poly-4-vinyl pyridine block copolymer P5722P (PS-b-P4VP 138,000-b-41,000 g/mol) was purchased from Polymer Source, Inc., Canada. Membranes were cast from polymer solutions containing 20 wt % copolymer in a mixture of 56 wt % *N*,*N*-dimethyl formamide (DMF), 24 wt % tetrahydrofuran (THF), and 0.15 wt % divalent metal acetate. The solvent was allowed to evaporate up to 20 s, and the film was immersed in water at room temperature.

Water Flux and pH Response. The water flux was measured under different pH values. Acid solutions were prepared with different concentrations of nitric acid. Basic solutions were prepared with ammonium hydroxide. The membranes (testing area ca. 5 cm^2) were tested in an Amicon cell at 1 bar.

The same procedure was repeated using a total of 0.5 wt % solution of polyethylene glycol (0.1 wt % of each 1500, 6000, 10 000, 15 000, 35 000 g/mol). Samples of the feed solution, retentate, and permeate were collected and analyzed by gel permeation chromatography. The analysis was performed by WEE-Solve, GmbH, Mainz. The samples were filtered with a 5 μm PTFE filter and injected into a 1 mL/min carrier solution of 0.1 mol/L $NaNO_3$ and 0.05 mol/L $NaHCO_3$, using Polymer Standards HEMA BIO 40, 1000 and SUPREMA 300 columns and a Gynkotek RI-71 refraction index detector.

Atomic Force Microscopy. The AFM analysis was performed using an ICON Veeco microscope.

Cryo-Field Emission Scanning Electron Microscopy. Low-temperature experiments were carried out using a Quorum PP2000T cryo-transfer system (Qurorum Technologies, Newhaven, UK) that was fitted to an FEI Nova Nano630 SEM with a field emission electron source and through-lens electron detectors.

A small amount of polymer solution was mounted between two rivets secured in a hole on an aluminum stub on the specimen holder. The sample holder, attached to a transfer rod, was then rapidly plunged into liquid nitrogen slush, transferred under vacuum to the preparation chamber precooled at −180 °C, and allowed to equilibrate for 10 min. The sample temperature was raised to −160 °C, and a fractured surface was obtained by hitting the top rivet with a knife and removing it from the top surface. The revealed fractured plane was sublimed at −90 °C for 5 min to eliminate any eventually

condensed ice. To avoid charging problems, the sample temperature was then reduced to −135 °C, and the sample was sputter-coated with gold−palladium for 90 s at 5 mA current in an argon atmosphere. The sample was then transferred to a SEM cryo-stage, which was held at −140 °C.

For observation of the nanoporous film surface morphology in solutions with different pH values, small pieces of membranes (approximately 2 mm × 5 mm) were immersed in aqueous solutions of pH 2.3 (adjusted with HCl) or pH 10.0 (adjusted with ammonium hydroxide) overnight. The excess water around the membranes was quickly removed using absorbent filter paper. To examine the top surface or the cross section, membranes were mounted either flat onto an aluminum stub using thin aluminum tape or vertically inside a machined slot aluminum stub using carbon paste. The stub was then secured on the specimen holder, rapidly plunged into liquid nitrogen slush, transferred under vacuum into a PP2000T preparation chamber precooled at −180 °C, and allowed to equilibrate for 10 min. The sample was then sublimed at −90 °C for 5 min to eliminate any condensed ice from the surface that was gained during the transfer. To avoid charging problems, the sample temperature was then reduced to −140 °C, and the sample was sputter-coated with gold−palladium for 60−120 s at 5−7 mA current in an argon atmosphere. The sample was then transferred to a SEM cryo-stage, which was held at −145 °C. The imaging was performed using an accelerating voltage of 2−5 kV and working distance of 5 mm.

Environmental Scanning Electron Microscopy. Wet membranes were analyzed using environmental SEM (FEI Quanta 200/600F series) with a gaseous secondary electron detector for imaging.

Dry membrane samples were mounted inside a depression on aluminum stubs, using aluminum tape. The samples thus mounted were wetted with aqueous solutions of pH 1.3 and 10.5, waiting 10−30 min before proceeding. Excess solution was then removed using an absorbent filter paper, and the stub was immediately transferred onto the precooled (2 °C) stage of the ESEM. Imaging was carried out at 3 kV with a working distance of 4−6 mm. Signal detection and image optimization were accomplished by varying the pressure (550−750 Pa) and humidity (60−100%) inside the ESEM chamber.

Transmission Electron Microscopy (TEM) Tomography. The membrane was embedded in low-viscosity epoxy resin (Agar R1165) and cured at 60 °C for 24 h. Ultrathin sections (80 nm) were prepared with an ultramicrotome (Leica EM UC6) and put on a carbon-coated copper grid. Images were obtained using a Tecnai 12 (FEI Company) operating at 120 keV. Tilt series were acquired by tilting the sample from −65° to +65° with a variable tilt increment according to the scheme proposed by Saxton *et al.*, starting with an increment of 2° at 0° tilt.[25] Tilt series for tomographic reconstruction were acquired using the FEI tomography package and reconstructed using SIRT procedures as implemented in Inspect 3D (FEI Company). Visualization and semiautomated segmentation were carried out using software tools implemented in the program Avizo (www.vsg3d.com).

Small-Angle X-ray Scattering (SAXS). SAXS analysis of PS-b-P4VP prepared with copper acetate was measured at beamline B1 at DORIS synchrotron in HASYLAB at DESY, in Hamburg. The experimental parameters are similar to those in ref 16. The length of the scattering vector is defined in the preceding report as $q = 4\pi \sin\theta/\lambda$, where θ is half of the scattering angle and λ is the wavelength of X-rays. The dry samples were measured under vacuum ($P < 10^{-4}$ mbar), and the wet samples were measured in quartz capillaries filled with solvent, which had either pH 2 (adjusted with HCl) or pH 9 (adjusted with NaOH). The first reflection in the dry membrane data and that in the pH 9 data were fitted with a power law background and Gaussian function after multiplying the intensities by q^2.

Supporting Information Available: (1) Low-magnification electron microscopy of ordered membrane surface with Cu(II); (2) transmission electron microscopy tomography videos of membranes prepared with Co(II); (3) SAXS analysis. This material is available free of charge *via* the Internet at http://pubs.acs.org.

Note Added after ASAP Publication: After this paper was published ASAP April 25, 2011, a correction was made to the affiliation for author Suzana P. Nunes. The revised version was published April 26, 2011.

REFERENCES AND NOTES

1. Jackson, E. A.; Hillmeyer, M. A. Nanoporous Membranes Derived from Block Copolymers: From Drug Delivery to Water Filtration. *ACS Nano* **2010**, *4*, 3548–3553.
2. Thurn-Albrecht, T.; Schotter, J.; Kastle, G. A.; Emley, N.; Shibauchi, T.; Krusin-Elbaum, L.; Guarini, K.; Black, C. T.; Tuominen, M. T.; Russell, T. P. Ultrahigh-Density Nanowire Arrays Grown in Self-Assembled Diblock Copolymer Templates. *Science* **2000**, *290*, 2126.
3. Yang, S.; Yang, J.-A.; Kim, E.-S.; Jeon, G.; Oh, E. J.; Choi, K. Y.; Hahn, S. K.; Kim, J. K. Single-File Diffusion of Protein Drugs Through Cylindrical Nanochannels. *ACS Nano* **2010**, *4*, 3817–3822.
4. Stuart, M. A. C.; Huck, W. T. S.; Genzer, J.; Muller, M.; Ober, C.; Stamm, M.; Sukhorukov, G. B.; Szleifer, I.; Tsukruk, V. V.; Urban, M.; *et al*. Emerging Applications of Stimuli-Responsive Polymer Materials. *Nat. Mater.* **2010**, *9*, 101–113.
5. Goposhetty, V.; Roiter, Y.; Tokarev, I.; Minko, S. Multiresponsive Biopolyelectrolyte Membrane. *Adv. Mater.* **2008**, *20*, 4588–4593.
6. Wandera, D.; Wickramasinghe, S. R.; Husson, S. M. Stimuli-Responsive Membranes. *J. Membr. Sci.* **2010**, *357*, 6–35.
7. Roy, D.; Cambre, J. N.; Smerlin, B. S. Future Perspectives and Recent Advances in Stimuli-Responsive Materials. *Prog. Polym. Sci.* **2010**, *35*, 278–301.
8. Yameen, B.; Ali, M.; Neumann, R.; Ensinger, W.; Knoll, W.; Azzaroni, O. Synthetic Proton-Gated Ion Channels via Single Solid-State Nanochannels Modified with Responsive Polymer Brushes. *Nano Lett.* **2009**, *9*, 2788–2793.
9. Schacher, F.; Ulbricht, M.; Müller, A. H. E. Self-Supporting Double Stimuli-Responsive Porous Membranes from Polystyrene-block-poly (*N*,*N*-dimethylaminoethyl methacrylate) Diblock Copolymers. *Adv. Funct. Mater.* **2009**, *19*, 1040–1045.
10. Ikkala, O.; Ten Brinke, G. Functional Materials Based on Self-Assembly of Polymeric Supramolecules. *Science* **2002**, *295*, 2407–2409.
11. Phillip, W. A.; O'Neill, B.; Rodwogin, M.; Hillmyer, M. A.; Cussler, E. L. Self-Assembled Block Copolymer Thin Films as Water Filtration Membranes. *ACS Appl. Mater. Interfaces* **2010**, *2*, 847–853.
12. Lee, J.-S.; Hirao, A.; Nakahama, S. Polymerization of Monomers Containing Functional Silyl Groups. 5. Synthesis of New Porous Membranes with Functional Groups. *Macromolecules* **1989**, *22*, 2602–2606.
13. Bates, F. S.; Fredrickson, G. H. Block Copolymer−Designer Soft Materials. *Phys. Today* **1999**, *52*, 32–38.
14. Hayward, R. C.; Pochan, D. J. Tailored Assemblies of Block Copolymers in Solution: It Is All About the Process. *Macromolecules* **2010**, *43*, 3577–3584.
15. Moughton, A. O.; O'Reilly, R. K. Using Metallo-Supramolecular Block Copolymers for the Synthesis of Higher Order Nanostructured Assemblies. *Macromol. Rapid Commun.* **2010**, *31*, 37–52.
16. Nunes, S. P.; Sougrat, R.; Hooghan, B.; Anjum, D. H.; Behzahd, A. R.; Zhao, L.; Pradeep, N.; Pinnau, I.; Vainio, U.; Peinemann, K.-V. Ultraporous Films with Uniform Nanochannels by Block Copolymer Micelles Assembly. *Macromolecules* **2010**, *43*, 8079–8085.
17. Spatz, J. P.; Sheiko, S.; Moeller, M. Ion-Stabilized Block Copolymer Micelles: Film Formation and Intermicellar Interaction. *Macromolecules* **1996**, *29*, 3220–3226.
18. Belfiore, L.; McCurdie, M. P. Reactive Blending via Metal-Ligand Coordination. *J. Polym. Sci., Part B: Polym. Phys.* **1995**, *33*, 105–124.
19. Frank, C. W.; Rogers, L. B. Infrared Spectral Study of Metal-Pyridine, -Substituted Pyridine, and -Quinoline Complexes in the 667−150 cm^{-1} Region. *Inorg. Chem.* **1966**, *5*, 615–622.
20. Brewer, D. G.; Wong, P. T. T. Studies of Metal Complexes of Pyridine Derivatives: The Effects of Coordination upon

Infrared Intensity of the Functional Group in β-Cyanopyridine. *Can. J. Chem.* **1966**, *44*, 1407–1419.
21. Belfiore, L. A.; McCurdie, M. P.; Das, P. K. Macromolecule-Metal Complexes: Ligand Field Stabilization and Thermophysical Property Modification. *Polymer* **2001**, *42*, 9995–10006.
22. Savariar, e. N.; Krishnamoorthy, K.; Thayumanavan, S. Molecular Discrimination inside Polymer Nanotubes. *Nat. Nanotechnol.* **2008**, *3*, 112–117.
23. Guo, X.; Zhang, L. J.; Wu, Z. M.; Qian, Y. Dissipative Particle Dynamics Studies on Microstructure of pH-Sensitive Micelles for Sustained Drug Delivery. *Macromolecules* **2010**, *43*, 7839–7844.
24. Nunes, S. P.; Peinemann, K.-V. Presently Available Membranes for Liquid Separation. In *Membrane Technology in the Chemical Industry*, 2nd ed.; Nunes, S. P.; Peinemann, K.-V., Eds.; Wiley-VCH: Weinheim, 2006; pp 15−38.
25. Saxton, W. O.; Baumeister, W.; Hahn, M. Three-dimensional Reconstruction of Imperfect Two-dimensional Crystals. *Ultramicroscopy* **1984**, *13*, 57–70.